Article

Mapping of Glaciers on Horseshoe Island, Antarctic Peninsula, with Deep Learning Based on High-Resolution Orthophoto

Mahmut Oğuz Selbesoğlu [1,*], Tolga Bakirman [2], Oleg Vassilev [3] and Burcu Ozsoy [4]

1   Department of Geomatics, Istanbul Technical University, 34469 Istanbul, Türkiye
2   Department of Geomatics, Yildiz Technical University, 34220 Istanbul, Türkiye
3   Bulgarian Antarctic Institute, 15 Tsar Osvoboditel Boulevard, 1504 Sofia, Bulgaria
4   Polar Research Institute, TÜBİTAK Marmara Research Center, 41470 Kocaeli, Türkiye
*   Correspondence: selbesoglu@itu.edu.tr

Abstract: Antarctica plays a key role in the hydrological cycle of the Earth's climate system, with an ice sheet that is the largest block of ice that reserves Earth's 90% of total ice volume and 70% of fresh water. Furthermore, the sustainability of the region is an important concern due to the challenges posed by melting glaciers that preserve the Earth's heat balance by interacting with the Southern Ocean. Therefore, the monitoring of glaciers based on advanced deep learning approaches offers vital outcomes that are of great importance in revealing the effects of global warming. In this study, recent deep learning approaches were investigated in terms of their accuracy for the segmentation of glacier landforms in the Antarctic Peninsula. For this purpose, high-resolution orthophotos were generated based on UAV photogrammetry within the Sixth Turkish Antarctic Expedition in 2022. Segformer, DeepLabv3+ and K-Net deep learning methods were comparatively analyzed in terms of their accuracy. The results showed that K-Net provided efficient results with 99.62% accuracy, 99.58% intersection over union, 99.82% precision, 99.76% recall and 99.79% F1-score. Visual inspections also revealed that K-Net was able to preserve the fine details around the edges of the glaciers. Our proposed deep-learning-based method provides an accurate and sustainable solution for automatic glacier segmentation and monitoring.

Keywords: Antarctica; deep learning; Horseshoe; glacier; orthophoto

1. Introduction

Antarctica has long been a hotspot for researchers, since it contains unique and valuable data that contribute to the better understanding of the past and shed light on the future of the Earth. This continent contains about 90% of the Earth's ice reserves and plays a key role in keeping the Earth's ecosystems in balance by providing heat balance throughout the oceans [1]. An increase in temperature causes a retreat of glaciers and a loss of glacial mass, leading to sea level rises and a loss of freshwater, which is of great importance to human beings.

Studies on this continent have predicted that the sea level change caused by the melting of the glaciers due to the deterioration of the radiation balance of the Earth will affect more than 1 billion people in the near future [2]. Therefore, monitoring the glaciers and revealing their movements caused by their own weight and the force of gravity is of great importance for climate change studies.

Remote sensing is an important supporting tool for monitoring climate change effects in terms of ice mass loss and sea level rises in the Antarctic. The first airplane reconnaissance flight for understanding Antarctica was carried out in the late 1920s. A milestone was achieved with Hubert Wilkins' first flight in 1929, which took off from Deception Island and revealed much of the northern part of the Antarctic Peninsula [3]. The mapping of Antarctica with aerial photography started only in the middle of the 20th century with the

Ronne Antarctic Research Expedition (RARE) [4]. After a long period of reconnaissance flights and aerial photogrammetry studies, satellite images have become a very important remote sensing source that has been available since the 1970's. Afterward, in the last few decades, satellite images and unmanned aerial vehicles have begun to be used for investigating the environmental effects in Antarctica.

The breakdown of the ecosystem due to the signs of climate change witnessed in the last decades in Antarctica has increased the importance of high-resolution data. Therefore, the important capability of UAV photogrammetry in generating high-resolution topographic maps has begun to be widely used for monitoring the changes in glacier structures. Many studies have been conducted for various purposes such as vegetation mapping [5], health assessments [6], landforms and soils [7], mosaics and DEM production [8–10]. Although there is a growing number of various imagery studies that have been conducted in Antarctica for many types of research, a comprehensive evaluation is missing for the segmentation of glaciers based on high-resolution data with the recent SotA deep learning architectures.

Researchers have proposed various methods in the literature for glacier mapping using remote sensing methods such as unsupervised classification, supervised classification, object-based classification, statistical-based classification and machine learning. Recent advances in artificial intelligence have emerged using deep learning in various computer vision applications including remote sensing. Some researchers have also focused on glacier mapping utilizing deep learning architectures. Nijhawan et al. [11] proposed a hybrid approach where they used CNNs for deep feature extraction from Landsat 8 imagery in order to delineate debris-covered glaciers in India. After running a principal component analysis (PCA) to select the features, the features were then assembled for classification with the random forest (RF) method. Baumhoer et al. [12] proposed a modified U-Net method to extract Antarctic glaciers using the Sentinel-1 imagery and TanDEM-X digital elevation models. Their study also focused on the extraction of coastlines along various study areas in the Antarctic. Xie et al. [13] developed GlacierNet based on SegNet for debris-covered glacier mapping in the Nepalese Himalayas and the central Karakoram region in Pakistan using Landsat 8 and ALOS DEM. In a separate study [14], they conducted a comparative assessment in the Himalayan region using GlacierNet, U-Net, Res-UNet, FC-DenseNet, R2Unet and DeepLabv3+, where DeepLabv3+ outperformed all the compared architectures. The authors then improved their model (GlacieNet2) by integrating data subsampling, CNN processing, terminus estimation improvement, and snow-covered accumulation zone estimation and tested it in the central Karakoram region in northern Pakistan [15]. Robson et al. [16] proposed a methodology that applied object-based image analysis (OBIA) on a predictions map derived by deep learning using Sentinel-1, Sentinel-2 and DEM. In this approach, OBIA required the determination of parameters and thresholds subjectively or experimentally. They also applied their methodology to 2 m resolution Pleiades imagery and a corresponding DEM in the Himalayas and the Chilean Andes. Yan et al. [17] integrated a U-Net architecture with a modified spatial–spectral attention module (SSAM) for glacier mapping in Xizang Province, China, using Sentinel-2 imagery. Khan et al. [18] developed a shallow architecture that consisted of the spatial-CNN and spectral-CNN methods to extract debris-covered glaciers in Pakistan from Sentinel-2 imagery. However, the authors mentioned that they had issues along the boundaries of classes. Kaushik et al. [19] proposed a fully connected feed-forward deep neural network called SGDNet for debris-covered glacier mapping across the Himalaya and Karakoram regions using freely available multi-source data, namely Sentinel-1, Sentinel-2, Landsat 8, ALOS DEM and slope. Even though various multi-source data were exploited, the method was not able to classify shaded areas sufficiently. Tian et al. [20] developed a channel-attention U-Net method with channel squeeze and excitation using Landsat 8 and SRTM DEM in the Pamir Plateau between Tajikistan and Afghanistan. Roberts-Pierel et al. [21] presented a GlacierCoverNet, encoder–decoder neural network architecture using features derived

from Landsat 4, Landsat 5, Landsat 7 and Landsat 8 for temporal glacier mapping between 1985–2020 in Alaska.

As can be seen in the literature review (Table 1), UAV imagery has not been exploited for glacier mapping with deep learning. Moreover, it was also observed that the recent deep learning methods have not been widely applied for glacier segmentation. The main purpose of this study was to reveal the performance of recent SotA deep learning approaches for the segmentation of glaciers using UAV imagery in Horseshoe Island, Antarctica. Our study's main contributions to the literature can be summarized as:

- A novel glacier segmentation dataset for deep learning was generated for the first time to date using UAV imagery in Antarctica.
- Recent state-of-the-art architectures and their performances, such as SegFormer, DeepLabv3+ and K-Net were employed and investigated for glacier segmentation.
- There has been no study to date in the literature that has focused on glacier mapping using aerial or UAV imagery utilizing deep learning
- The extraction of small, discontinuous and shaded glaciers was efficiently dealt with in the K-Net architecture.
- Glacier mapping has been hardly applied in the Antarctica region.

Table 1. Highlights and shortcomings of deep learning methods used for glacier segmentation in the literature.

Study	Method	Highlights	Shortcomings
Nijhawan, et al. [11]	3 CNNS + PCA + RF + post-processing	Better results than SVM, ANN and RF.	Manual feature selection.
Baumhoer, et al. [12]	Modified U-Net + post-processing	Extracts coastlines along with glacier and ice shelf fronts.	Based on only radar imagery.
Xie, et al. [13]	GlacierNet CNN + post-processing	The use of morphometric parameters increases boundary detection performance.	Multi-source data acquired at different times caused errors.
Xie, et al. [15]	GlacierNet2 CNN	Improved accuracy compared to GlacierNet and DeepLabv3+.	Compared with a single state-of-the-art method.
Robson, et al. [16]	CNN + OBIA + post-processing	Based on freely available remote sensing data.	The parameters and thresholds were chosen subjectively.
Yan, et al. [17]	Modified U-Net	Increased accuracy with SSAM.	Outperformed the original U-Net by only 1 percent.
Khan, et al. [18]	Spatial and spectral CNNS + FCN + post-processing	A shallow network was developed.	Errors along the boundary among the classes.
Kaushik, et al. [19]	Six-layered CNN	Based on freely available remote sensing data.	Areas with shadows could not be sufficiently classified.
Tian, et al. [20]	Channel-attention U-Net + CRF post-processing	Better results than U-Net and GlacierNet.	Post-processing may result in the underestimation of glaciers.
Roberts-Pierel, et al. [21]	ResNeSt-101 + PSPNet	Better glacier outlines than Randolph Glacier Inventory 6.0 data [22].	Limited ability to accurately map small, discontinuous and shaded glaciers

In the next section, the UAV flights carried out during the Sixth Turkish Antarctic Expedition are described including detailed information on the UAV data analysis. Afterward, the segmentation methodology of the models is given. Then, the maps created using the proposed deep learning approaches are interpreted in terms of their accuracy with a comparative assessment. In the last section, the article is concluded with the major findings of the study.

2. Materials and Methods

The focus of this study was dedicated to the development of accurate segmentation models based on different deep learning approaches in order to determine glacial areas. The main objective was to detect and map the presence/absence of glaciers in each pixel based on recent deep-learning approaches by the proposed method. For this purpose, orthophoto of the center of Horseshoe Island were generated based on UAV photogrammetry to monitor the snow/ice fields next to the Turkish Scientific Research Station. The Turkish Scientific Research Station is located on Horseshoe Island, which is one of the islands in Marguerite Bay in the Antarctic Peninsula. During the 6th National Antarctic Science Expedition, this study was carried out at a particular test location on Horseshoe Island (between latitude 67°49′57.46 and longitude 67°13′3.40) (Figure 1).
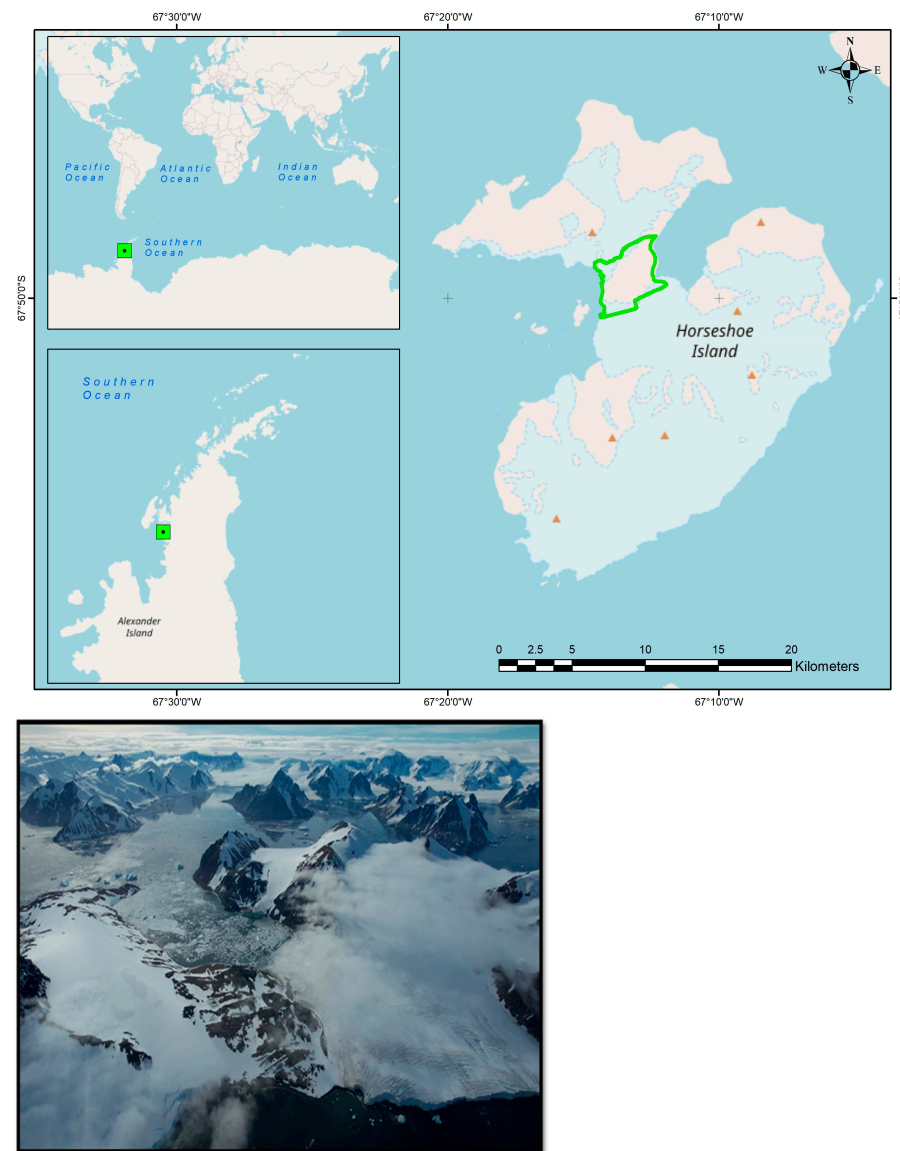
Figure 1. Horseshoe Island, Antarctica. The green squares in the small maps show the location of Horseshoe Island. The green polyline shows the boundary of the study area on the island. The orange triangles indicate the elevation extremes of the island.

The island's northern part is mostly covered by an ice cap, and the middle part is covered by glacial and periglacial landforms [23]. Therefore, the middle part of the island was chosen since the glacial and landform coverage was more extensive than in the other parts of the island (Figure 1). The stages involved in the execution of this study involved

establishing ground control points (GCPs) in the research region, performing a flight plan from a fixed height above the takeoff point, processing the photogrammetric data obtained in an office setting and creating orthophotos and DEMs in the Pix4Dmapper program (Figure 2). In order to produce the orthophotos whilst ensuring the accuracy requirements, 14 homogenously distributed GCPs were placed with double-laminated paper (30×30 cm) firmly fixed by anchor bolts (brass inserts and stainless-steel M8 bolts) on 12th of February. The GCP marks were distributed from the west beach (camp side) to the east beach. The coordinate measurement of the GCPs was performed in the RTK format with an Emlid Receiver, which could retrieve data in two frequencies (L1/L2) [24]. The base antenna location was measured from the Turkish permanent station on Horseshoe Island (station name: TUR1).
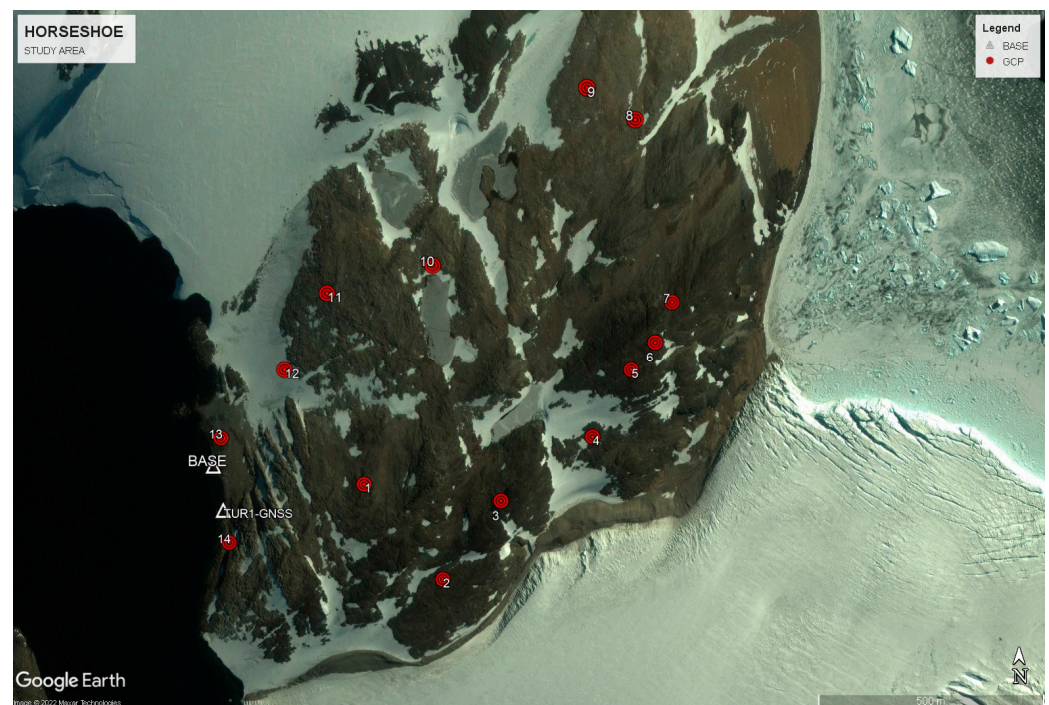
Figure 2. Distribution of ground control points (GCP, 1–14), Base GNSS Station and Turkish Permanent GNSS Station (TUR1) in the study area.

The first flight was conducted on 14th of February at the area of the west beach, covering an area of 1.32 km^2. The flight was performed at 90 m above the take-off point. The achieved average GSD was 2.72 cm/pixel. The second flight was conducted on 16th of February, covering an area from the lake area to the eastern beach—in total 3.15 km^2. The flight was performed at 80 m above the take-off point. All the flights were performed with a DJI Phantom 4 Pro equipped with a Topodrone PPK set. The cameras resolution was 20 MP with a 1-inch (13.2–8.8 mm) sensor and a mechanical shutter. The Map pilot flight-planning software was used for the photogrammetric survey. The number of collected images was 3200 The average achieved GSD was 3.15 cm/pixel for the second flight. The photogrammetric processes were carried out by the image input system WGS 84 and the project output system WGS 84/UTM 19S. The distance between the base antenna location and the TUR1 GNSS station was approximately 200 m. The orthoimages were created with an 8-bit pixel depth. In the processing step, orthomosaic and digital surface model (DSM) were produced in the Pix4Dmapper software based on the Structure from Motion (SfM) algorithm (Figure 3).

(**a**)   (**b**)
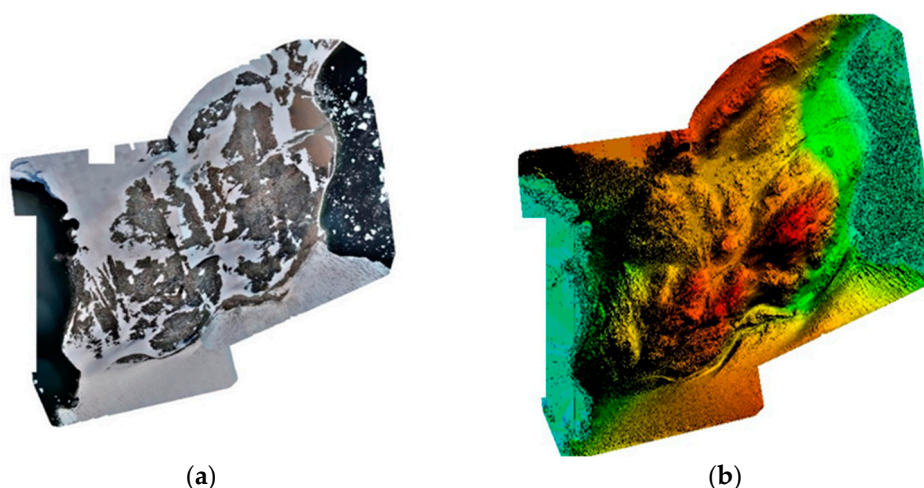
Figure 3. (**a**) Orthomosaic. (**b**) DEM.

The RMSE of the orthophoto based on 4 check points was found to be 2.78 cm on average, and this is given separately for 3 axes in Table 2.

Table 2. Flight parameters and positioning accuracy.

Number of Images	5393 Images
Average ground sampling distance (GSD)	3.00 cm
Area covered	2668 km^2
Georeferencing	14 3D control points
RMS error (cm) [X, Y, Z]	1.30, 0.97, 2.27

In order to create glacier labels on the produced orthophotos, ISODATA unsupervised classification [25] was performed on the orthoimage. Although the unsupervised classification process was able to extract the general borders of the major areas, the algorithm produced countless noisy small patches. Therefore, the whole images were checked manually in terms of quality in order to edit the extracted borders and clean the noise. The orthoimage and their corresponding label raster were split in to 512×512-pixel-sized image patches (Figure 4). We also applied the vertical flip, horizontal flip and shift–scale–rotate augmentation techniques. Finally, the dataset was split into training, validation and test sets that consisted of 5980, 1291 and 1437 image patches, respectively.
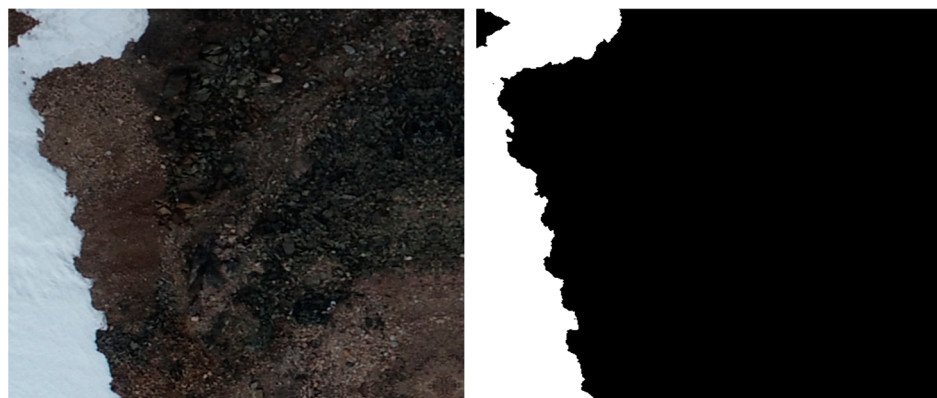
Figure 4. A sample image patch (512×512) from the dataset and the corresponding label (white: glacier; black: background).

In this study, we utilized three recent state-of-the-art deep learning architectures, namely DeepLabv3+, SegFormer and K-Net. The original DeepLab [26] architecture used

the Atrous algorithm and a fully connected conditional random field (CRF) algorithm at the pixel level to control the resolution of the feature maps. In the second version of the architecture [27], Atrous convolutions and Atrous spatial pyramid pooling (ASPP) modules were implemented in order to segment objects at multiple scales. DeepLabv3 [28] improved upon the Atrous convolutions and ASPP with various rates and batch normalization layers. The authors also augmented ASPP with image-level features in order to capture the global context and remove the DenseCRF post-processing module, since the improved architecture was able to segment objects efficiently without CRF. In the final version of the architecture, DeepLabv3+ [29] used DeepLabv3 as an encoder module, and a decoder module was proposed in order to capture sharper object boundaries. Furthermore, the Xception model was adapted for segmentation, and the authors also implemented a depthwise separable convolution to both the ASPP module and the decoder module for a better and robust network.

SegFormer [30] combines a hierarchically structured transformer encoder with multiscale features and lightweight multilayer perceptron (MLP) decoders. The proposed transformer-based encoder did not exploit the interpolation of positional codes and, therefore, could adapt to different image resolutions during inference. The hierarchical feature of the encoder allowed the creation of multi-level high-resolution fine features and low-resolution global features. On the other hand, the MLP decoder was able to unify local and global attention by gathering information from different layers. The authors developed Mix Transformer (MiT) encoders, which were based on ViT with various sizes starting from MiT-B0 to MiT-B5. In this study, we implemented the MiT-B5 model for the best performance.

The K-Net [31] architecture is based on a set of randomly initialized convolutional kernels that can be used for semantic, instance and panoptic segmentation. The kernels are learned through semantic kernels for semantic categories. Convolutions are performed by the semantic kernels in order to achieve the corresponding segmentation predictions. The kernels are dynamically updated globally in order to improve the kernels in terms of their discriminative ability. For object detection, the authors employed a bipartite matching strategy that builds a one-to-one mapping between the kernels and instances in an image. Additionally, the K-Networks architecture is based on masks and does not require bounding boxes, which makes non-max suppression redundant.

3. Results and Discussion

In this study, we aimed to extract glacier areas from very-high-resolution orthoimagery using the SegFormer, DeepLabv3+ and K-Net architectures. The deep learning models were implemented using the Python MMSegmentation deep learning library [32] using a PyTorch backend. The accuracy assessment results calculated with the test dataset, which consisted of 1437 image patches, are given in Table 3 for all the deep learning models. Table 3 shows that all the deep learning models performed efficiently and obtained around 99% for all the accuracy metrics. However, it can be seen that K-Net robustly outperformed SegFormer and DeepLabv3+ in terms of all the accuracy metrics except recall. The SegFormer model, which utilizes transformers for feature extraction, seemed to be inferior to DeepLabv3+ and K-Net, which utilize atrous convolutions and convolution kernels, respectively.

Table 3. Accuracy assessment results. The best result for each accuracy metric is underlined.

	Segformer	DeepLabv3+	K-Net
Accuracy	98.85%	99.18%	<u>99.62%</u>
IoU	98.73%	99.09%	<u>99.58%</u>
Precision	98.89%	99.37%	<u>99.82%</u>
Recall	<u>99.83%</u>	99.72%	99.76%
F1-Score	99.36%	99.54%	<u>99.79%</u>

The prediction results from the test dataset are given in Figure 5. Although there were no huge differences between the deep learning models considering the accuracy

metrics, significant variations were noticed, especially in the transitions between land and glacier. Both SegFormer and Deeplabv3+ models could extract the general structure of the glaciers. However, they both seemed to fail to preserve the fine details around the edges. On the other hand, K-Net performed efficiently in terms of both the general structure and the fine details of the glaciers. As shown in Figure 5a,c, SegFormer was not able to distinguish small-sized rocks within the glaciers. DeepLabv3+ could detect some of these rocks, however it still failed in terms of the tiny ones, while K-Net was able to detect them all with no dependence on the size. Figure 5b shows an example with a more regular transition between glacier and rock. SegFormer and DeepLabv3+ smoothed this transition, while K-Net was able to preserve small fluctuations. As shown in Figure 5d, similar to its performance with small and tiny rocks, SegFormer could not extract small-size glaciers, while DeepLabv3+ could only predict some of them. K-Net still seemed to be successful for the small- and even tiny-sized glaciers that were surrounded by rocks. In the cases of shadows (Figure 5e), generally, all the models seemed to perform efficiently. However, SegFormer and DeepLabv3+ produced some false-positives and false-negatives, respectively. Overall, all the architectures were able to extract glaciers efficiently; however, it was evident that K-Net was superior to Deeplabv3+ and Segformer in terms of preserving boundaries and extracting small-sized glaciers. This was the main reason that K-Net stepped forward in terms of accuracy assessment (Table 3).
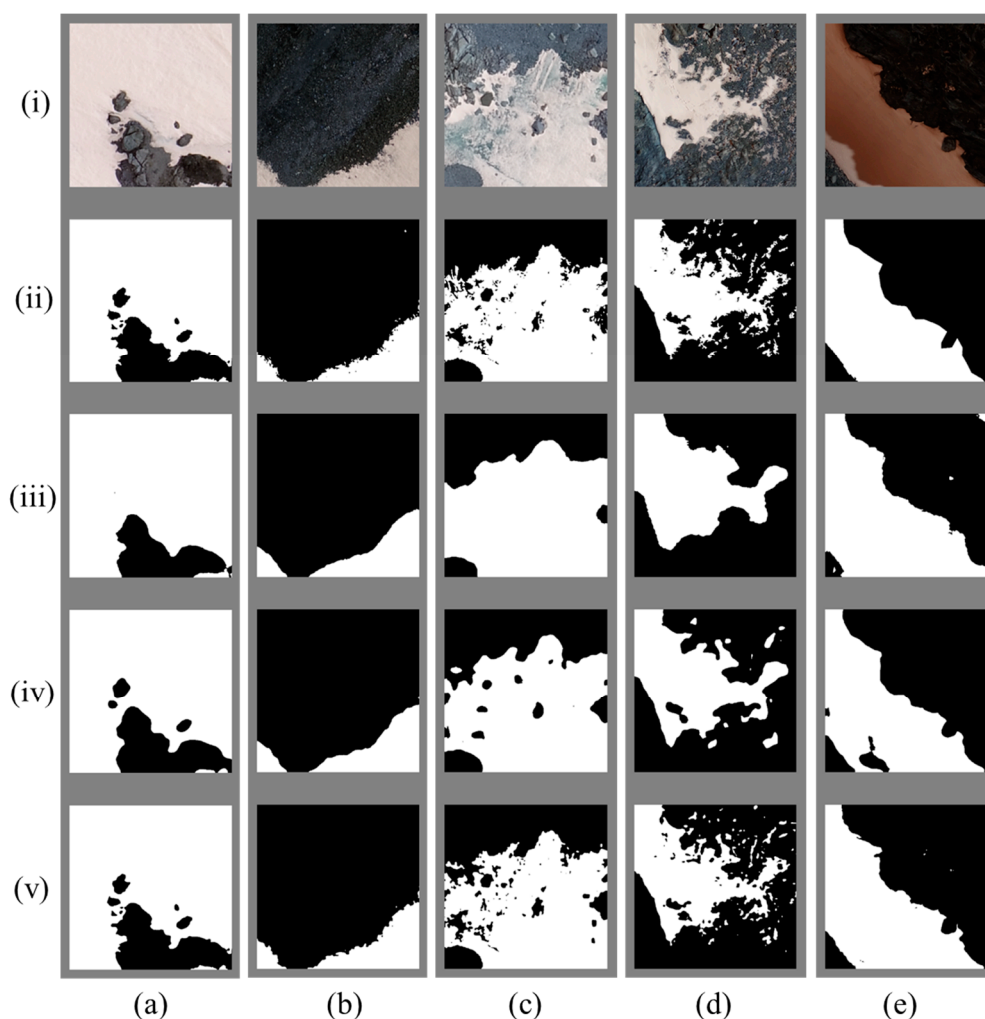
Figure 5. Prediction results from 5 images with different details (**a**–**e**) for all DL models. (**i**): test image, (**ii**): label, (**iii**): SegFormer result, (**iv**): DeepLabv3+ result, (**v**): K-Net result.

There are similar studies in the literature that have focused on pixel-level glacier segmentation with deep learning architectures. Yan et al. [17] have applied SSAM with a U-Net architecture on Sentinel-2 imagery bands with 10 m and 20 m geometric resolutions for glacier mapping. They resampled all Sentinel-2 bands to 10 m and obtained 96.87%, 98.70% and 97.88% results for accuracy, precision and recall, respectively. With this modification, they outperformed the original U-Net architecture by only about 1%. Tian et al. [20] used a channel-attention U-Net architecture on a data combination of Landsat 8 and SRTM DEM for the same purpose. They resampled the Landsat 8 imagery to 15 m and obtained false color imagery. The authors also resampled SRTM DEM using a nearest-neighbor algorithm in order to match it with the Landsat 8 image. In their study, they obtained accuracy, recall and F1-score values of 97.74%, 89.09% and 89.46%, respectively. Even though the applied conditional random field (CRF) post-processing increased the accuracy it also caused glaciers to be underestimated. Roberts-Pierel et al. [21] implemented their proposed GlacierCoverNet on Alaska IfSAR 5 m DEM and five optical indices calculated from 30 m Landsat 4, Landsat 5, Landsat 7 and Landsat 8 images. The authors applied their method in two sub-regions and obtained results of 94% and around 86% for all the calculated accuracy metrics using point-based validation, which is generally not preferred in deep learning applications. While their study presented temporal changes of around 35 years, their method failed to extract small and discontinuous glaciers. The accuracy metrics used in the similar studies in the literature (Table 4) showed that our proposed deep learning solution provided an efficient, accurate and rapid solution for glacier mapping considering the obtained accuracy values.

Table 4. Accuracy results from similar studies in the literature.

Study	Data	Resolution	Location	Accuracy	Precision	Recall	F1-Score
Yan, et al. [17]	Sentinel-2	10 m	Xizang Province, China	96.87%	98.70%	97.88%	N/A
Tian, et al. [20]	Landsat 8	15 m	Pamir Plateau, Tajikistan	97.74%	N/A	89.09%	89.46%
Roberts-Pierel, et al. [21]	Landsat 4, 5, 7, 8	30 m	Southern Alaska	N/A	94.00%	94.00%	94.00%
			Brooks Range, Alaska	N/A	87.00%	86.00%	86.00%
Ours (K-Net)	UAV	3 cm	Horseshoe Island, Antarctica	99.62%	99.82%	99.76%	99.79%

4. Conclusions

Antarctica is the most vulnerable region to global warming and climate change, which is the primary concern of human beings. Recent studies have revealed that the melting of glaciers will affect more than 1 billion people living in coastal zones in the future [2].

SotA monitoring solutions are demanded by decision makers and marine environment authorities to obtain accurate, reliable, efficient, temporal and sustainable data. As indicated in this study, glacier mapping was essential for our study area located in the west coast of the Antarctic Peninsula.

In the last decades, with the increasing demand for monitoring studies due to the effects of global climate change, segmentation of the important physical features of the Earth's surface based on deep learning has become a powerful tool. Considering the advantages and disadvantages of the conventional methods, deep learning approaches provide solutions for the segmentation of glacial landforms in a timely and cost-effective way. Therefore, the main purpose of this study was to investigate the ability of recent deep learning approaches in order to produce more accurate mapping applications in terms of time, resolution and cost, especially in Antarctica, to aid in achieving a climate-change-resilient environment.

In this study, we realized an assessment of recent SotA deep learning models for automatic glacier segmentation in the Antarctic using very-high-resolution UAV images. One of the main outcomes of this study was the novel glacier segmentation dataset obtained

for Horseshoe Island. To the best of our knowledge, this was the first glacier segmentation dataset that has benefitted from UAV imagery in the Antarctic region.

In this study, we conducted experiments using SegFormer, DeepLabv3+ and K-Net on our created dataset. These architectures were implemented for the first time in the literature for glacier segmentation. The investigations showed that the K-Net architecture produced the best accuracy metrics and the best visual results among the experiments. The results showed that the proposed solutions provided highly accurate results compared to the current literature. The proposed deep-learning-based workflow demonstrated that it was possible to provide the high-resolution mapping of a glacier using a deep learning approach based on high-resolution orthophotos obtained with a UAV survey. The advantage of using high-resolution orthophotos is that they could provide a decrease in the uncertainty related to pixel size. Therefore, more detailed features could be identified using this proposed method that could speed up the delineation of glacier boundaries with higher resolutions than using satellite imagery. For future studies, we aim to improve our proposed solution for temporal glacier monitoring in the Antarctic to combat climate-change-related environmental challenges. In this context, we aim to expand our dataset to include more classes such as water, melting ice, land, etc., in order to perform a more comprehensive deep-learning-based segmentation. In addition, based on the high-resolution glacier map obtained by the proposed method, the resulting map would help in detecting permafrost areas for future studies.

Author Contributions: Conceptualization, M.O.S., T.B. and B.O.; Methodology, M.O.S., T.B. and O.V.; Software, M.O.S. and T.B.; validation, M.O.S., T.B. and O.V.; formal analysis, M.O.S., T.B. and O.V.; investigation, M.O.S. and T.B.; resources, M.O.S. and O.V.; data curation, M.O.S. and T.B.; writing— original draft preparation, M.O.S. and T.B.; writing—review and editing, M.O.S., T.B. and O.V.; visualization, M.O.S., T.B. and O.V.; supervision, M.O.S. and B.O.; project administration, M.O.S.; funding acquisition, M.O.S. and B.O. All authors have read and agreed to the published version of the manuscript.

Data Availability Statement: The datasets generated and/or analyzed during the current study will be available from the corresponding author upon reasonable request after the completion of the project.

Conflicts of Interest: The authors declare no conflict of interest.

References

1. Turner, J.; Barrand, N.E.; Bracegirdle, T.J.; Convey, P.; Hodgson, D.A.; Jarvis, M.; Jenkins, A.; Marshall, G.; Meredith, M.P.; Roscoe, H.; et al. Antarctic climate change and the environment: An update. *Polar Rec.* **2014**, *50*, 237–259. [CrossRef]
2. Kulp, S.A.; Strauss, B.H. New elevation data triple estimates of global vulnerability to sea-level rise and coastal flooding. *Nat. Commun.* **2019**, *10*, 1–12.
3. Wilkins, H. The Wilkins-Hearst Antarctic Expedition, 1928-1929. *Geogr. Rev.* **1929**, *19*, 353–376. [CrossRef]
4. Pope, A.; Rees, W.G.; Fox, A.J.; Fleming, A. Open access data in polar and cryospheric remote sensing. *Remote Sens.* **2014**, *6*, 6183–6220. [CrossRef]
5. Lucieer, A.; Robinson, S.A.; Turner, D. Unmanned aerial vehicle (UAV) remote sensing for hyperspatial terrain mapping of Antarctic moss beds based on structure from motion (SfM) point clouds. In Proceedings of the 34th International Symposium on Remote Sensing of Environment, Sydney, Australia, 10–15 April 2011.
6. Turner, D.; Lucieer, A.; Malenovský, Z.; King, D.; Robinson, S.A. Assessment of Antarctic moss health from multi-sensor UAS imagery with Random Forest Modelling. *Int. J. Appl. Earth Obs. Geoinf.* **2018**, *68*, 168–179. [CrossRef]
7. Mergelov, N.; Dolgikh, A.; Shorkunov, I.; Zazovskaya, E.; Soina, V.; Yakushev, A.; Fedorov-Davydov, D.; Pryakhin, S.; Dobryansky, A. Hypolithic communities shape soils and organic matter reservoirs in the ice-free landscapes of East Antarctica. *Sci. Rep.* **2020**, *10*, 10277. [CrossRef]
8. Aykut, N.O. The Research for Usability of Unmanned Aerial Vehicles in Coastal Line Determination. *Geomatik* **2019**, *4*, 141–146.
9. Bliakharskii, D.; Florinsky, I.; Skrypitsyna, T. Modelling glacier topography in Antarctica using unmanned aerial survey: Assessment of opportunities. *Int. J. Remote Sens.* **2019**, *40*, 2517–2541. [CrossRef]

10. Lamsters, K.; Karušs, J.; Krievāns, M.; Ješkins, J. High-resolution orthophoto map and digital surface models of the largest Argentine Islands (the Antarctic) from unmanned aerial vehicle photogrammetry. *J. Maps* **2020**, *16*, 335–347. [CrossRef]
11. Nijhawan, R.; Das, J.; Balasubramanian, R. A hybrid CNN+ random forest approach to delineate debris covered glaciers using deep features. *J. Indian Soc. Remote Sens.* **2018**, *46*, 981–989. [CrossRef]
12. Baumhoer, C.A.; Dietz, A.J.; Kneisel, C.; Kuenzer, C. Automated extraction of antarctic glacier and ice shelf fronts from sentinel-1 imagery using deep learning. *Remote Sens.* **2019**, *11*, 2529. [CrossRef]
13. Xie, Z.; Haritashya, U.K.; Asari, V.K.; Young, B.W.; Bishop, M.P.; Kargel, J.S. GlacierNet: A deep-learning approach for debris-covered glacier mapping. *IEEE Access* **2020**, *8*, 83495–83510. [CrossRef]
14. Xie, Z.Y.; Asari, V.K.; Haritashya, U.K. Evaluating deep-learning models for debris-covered glacier mapping. *Appl. Comput. Geosci.* **2021**, *12*, 100071. [CrossRef]
15. Xie, Z.; Haritashya, U.K.; Asari, V.K.; Bishop, M.P.; Kargel, J.S.; Aspiras, T.H. GlacierNet2: A Hybrid Multi-Model Learning Architecture for Alpine Glacier Mapping. *Int. J. Appl. Earth Obs. Geoinf.* **2022**, *in press*.
16. Robson, B.A.; Bolch, T.; MacDonell, S.; Hölbling, D.; Rastner, P.; Schaffer, N. Automated detection of rock glaciers using deep learning and object-based image analysis. *Remote Sens. Environ.* **2020**, *250*, 112033. [CrossRef]
17. Yan, S.; Xu, L.; Yu, G.; Yang, L.; Yun, W.; Zhu, D.; Ye, S.; Yao, X. Glacier classification from Sentinel-2 imagery using spatial-spectral attention convolutional model. *Int. J. Appl. Earth Obs. Geoinf.* **2021**, *102*, 102445. [CrossRef]
18. Khan, A.A.; Jamil, A.; Hussain, D.; Ali, I.; Hameed, A.A. Deep learning-based framework for monitoring of debris-covered glacier from remotely sensed images. *Adv. Space Res.* **2022**, *in press*. [CrossRef]
19. Kaushik, S.; Singh, T.; Bhardwaj, A.; Joshi, P.K.; Dietz, A.J. Automated Delineation of Supraglacial Debris Cover Using Deep Learning and Multisource Remote Sensing Data. *Remote Sens.* **2022**, *14*, 1352. [CrossRef]
20. Tian, S.; Dong, Y.; Feng, R.; Liang, D.; Wang, L. Mapping mountain glaciers using an improved U-Net model with cSE. *Int. J. Digit. Earth* **2022**, *15*, 463–477. [CrossRef]
21. Roberts-Pierel, B.M.; Kirchner, P.B.; Kilbride, J.B.; Kennedy, R.E. Changes over the Last 35 Years in Alaska's Glaciated Landscape: A Novel Deep Learning Approach to Mapping Glaciers at Fine Temporal Granularity. *Remote Sens.* **2022**, *14*, 4582. [CrossRef]
22. RGI Consortium. *Randolph Glacier Inventory—A Dataset of Global Glacier Outlines, Version 6 [Data Set]*; National Snow and Ice Data Center: Boulder, CO USA, 2017. Available online: https://doi.org/10.7265/4m1f-gd79 (accessed on 12 October 2022).
23. Yıldırım, C. Geomorphology of Horseshoe Island, Marguerite Bay, Antarctica. *J. Maps* **2020**, *16*, 56–67. [CrossRef]
24. Padró, J.-C.; Muñoz, F.-J.; Planas, J.; Pons, X. Comparison of four UAV georeferencing methods for environmental monitoring purposes focusing on the combined use with airborne and satellite remote sensing platforms. *Int. J. Appl. Earth Obs. Geoinf.* **2019**, *75*, 130–140. [CrossRef]
25. Ball, G.H.; Hall, D.J. *ISODATA, a Novel Method of Data Analysis and Pattern Classification*; Stanford Research inst Menlo Park: Menlo Park, CA, USA, 1965.
26. Chen, L.-C.; Papandreou, G.; Kokkinos, I.; Murphy, K.; Yuille, A.L. Semantic image segmentation with deep convolutional nets and fully connected crfs. *arXiv* **2014**, arXiv:1406.2661.
27. Chen, L.-C.; Papandreou, G.; Kokkinos, I.; Murphy, K.; Yuille, A.L. Deeplab: Semantic image segmentation with deep convolutional nets, atrous convolution, and fully connected crfs. *IEEE Trans. Pattern Anal. Mach. Intell.* **2017**, *40*, 834–848. [CrossRef]
28. Chen, L.-C.; Papandreou, G.; Schroff, F.; Adam, H. Rethinking atrous convolution for semantic image segmentation. *arXiv* **2017**, arXiv:1706.05587.
29. Chen, L.-C.; Zhu, Y.; Papandreou, G.; Schroff, F.; Adam, H. Encoder-decoder with atrous separable convolution for semantic image segmentation. In Proceedings of the European Conference on Computer Vision (ECCV), Munich, Germany, 8–14 September 2018; pp. 801–818.
30. Xie, E.; Wang, W.; Yu, Z.; Anandkumar, A.; Alvarez, J.M.; Luo, P. SegFormer: Simple and efficient design for semantic segmentation with transformers. *Adv. Neural Inf. Process. Syst.* **2021**, *34*, 12077–12090.
31. Zhang, W.; Pang, J.; Chen, K.; Loy, C.C. K-net: Towards unified image segmentation. *Adv. Neural Inf. Process. Syst.* **2021**, *34*, 10326–10338.
32. MMSegmentation Contributors. OpenMMLab Semantic Segmentation Toolbox and Benchmark [Computer Software]. 2020. Available online: https://github.com/open-mmlab/mmsegmentation (accessed on 15 November 2022).